



Cite this: *Nanoscale Adv.*, 2019, 1, 1013

# Wealth from waste: *M. acuminata* peel waste-derived magnetic nanoparticles as a solid catalyst for the Henry reaction†

Gunindra Pathak, Kalyani Rajkumari and Samuel Lalthazuala Rokhum \*

Biosynthesis of nanoparticles by exploiting different plant materials has become a matter of great interest in recent years and is considered as a green technology as it does not involve any harmful and toxic chemicals in the synthetic procedure. In this paper, we report a novel one-pot *M. acuminata* peel ash extract mediated bio-synthesis of basic iron oxide nanoparticles (MAPAE@Fe<sub>3</sub>O<sub>4</sub>). The nanoparticles were fully characterized by different analytical techniques such as XRF, IR, XRD, XPS, SEM, TEM, VSM and TGA. The synthesized nanoparticles exhibited high basicity due to the presence of metal oxides, primarily basic K<sub>2</sub>O in the outer layer of Fe<sub>3</sub>O<sub>4</sub> surfaces, and showed good catalytic activity for the synthesis of β-nitroalcohol via the Henry reaction at room temperature under solvent-free conditions. The catalyst was separated from the reaction medium by simply applying an external bar magnet making the process economical and less labor intensive. Furthermore, the catalyst can be reused up to the 4<sup>th</sup> cycle without much loss of its activity.

Received 31st October 2018  
Accepted 20th November 2018

DOI: 10.1039/c8na00321a

rsc.li/nanoscale-advances

## 1 Introduction

The Henry reaction is one of the most important carbon–carbon bond forming reactions and has significant applications in organic synthesis. The product 2-nitroalcohol can act as an intermediate in the formation of nitroalkenes, α-nitroketones, and β-amino alcohol derivatives, and synthesis of chiral ligands and some biologically active compounds.<sup>1,2</sup> It can also be easily transformed into other chiral building blocks by oxidation, reduction, the Nef reaction or a nucleophilic displacement reaction due to chemical versatility of the nitro group present in the product molecule.<sup>3</sup> Therefore, continuous efforts have been devoted to developing a simple and mild catalytic system for the Henry reaction. However, the use of a conventional base resulted in side products along with the desired β-nitroalcohol and this limitation is overcome by the use of various functionalized metal complexes and organocatalysts.<sup>4–7</sup> Additionally, the problem of toxicity, catalyst recoverability and reusability and high cost cannot be ignored. Therefore, to address these difficulties further development was needed to provide green and productive methodologies.

During the last few years, Fe<sub>3</sub>O<sub>4</sub> magnetic nanoparticles have been getting considerable attention from researchers due to their (i) high catalytic activity, (ii) thermostability, (iii) easy

magnetic recoverability and recyclability, *etc.* Besides these, cost effectiveness, low toxicity, bio-compatibility and high surface area to volume ratios are also some great advantages of Fe<sub>3</sub>O<sub>4</sub> magnetic nanoparticles.<sup>8–11</sup> Iron oxide magnetic nanoparticles have been extensively used in various fields of science and technology such as magnetic resonance imaging, targeted drug delivery systems, data storage, wastewater treatment, catalysis, *etc.*<sup>12–16</sup> Furthermore, an Fe<sub>3</sub>O<sub>4</sub> magnetic nanocatalyst is considered as a suitable support for the preparation of a highly active metal catalyst as this metal catalyst on its surface prevents agglomeration of catalyst particles during separation which increases the catalyst imperishability.<sup>17</sup> There are various methods for synthesizing Fe<sub>3</sub>O<sub>4</sub> magnetic nanoparticles, among them co-precipitation methods have been recognized as the most efficient and simplest. Beside this, other methods like the sol-gel method,<sup>18</sup> hydrothermal techniques,<sup>19</sup> forced hydrolysis,<sup>20</sup> microemulsion techniques,<sup>21</sup> sono-chemical methods,<sup>22</sup> and electrochemical routes<sup>23</sup> are also extensively used. However, these methods are very expensive, outdated and potentially hazardous to the environment due to the use of toxic chemicals and solvents like sodium borohydride, hydrazine, carbon monoxide, sodium citrate, dimethylformamide, *etc.*<sup>24</sup> Therefore, to deal with these limitations, green- or biosynthesis of Fe<sub>3</sub>O<sub>4</sub> nanoparticles has been chosen as an environmental friendly, low cost alternative to these chemical methods. There are many methods available for synthesizing biogenic iron oxide nanoparticles by using various biological materials and organisms like bacteria,<sup>25</sup> fungi,<sup>26</sup> yeasts,<sup>27</sup> plant leaves,<sup>28</sup> fruit peel,<sup>29</sup> *etc.* However, a brief study of the literature reveals that the use of naturally available *M. acuminata* banana peel ash extracts has not been investigated for the synthesis of Fe<sub>3</sub>O<sub>4</sub> nanoparticles.

Department of Chemistry, National Institute of Technology, Silchar, Silchar-788010, Assam, India. E-mail: rokhum@che.nits.ac.in; Fax: +91 3842-224797; Tel: +91 3842 242915

† Electronic supplementary information (ESI) available: XPS, TEM, and EDX of the recovered MAPAE@Fe<sub>3</sub>O<sub>4</sub>, and <sup>1</sup>H and <sup>13</sup>C NMR spectra of the synthesized compounds. See DOI: 10.1039/c8na00321a



Herein, we report first successful one pot synthesis of basic  $\text{Fe}_3\text{O}_4$  magnetic nanoparticles using *M. acuminata* peel ash extracts as they provides a strong basic medium for co-precipitation procedures. Banana peel is considered as an agro waste product produced in large amounts annually by food processing industries across the world.<sup>30</sup> *M. acuminata* peel ash contains oxides of some metals, like potassium, calcium, silicon, *etc.*, that can be used as a base in many chemical transformations.<sup>31</sup> Waste banana peel has been utilized in numerous applications like organic fertilizers, catalysts for biodiesel production, biosorbents for removal of hazardous metal and dyes from wastewater, biotechnology related processes, *etc.*<sup>30,32</sup> Therefore researchers are very much motivated to come up with a methodology/process to reuse this waste banana peel to produce some environmentally useful and profitable products such that valorization of this waste product can contribute its removal from the environment avoiding its handling as a solid waste material. Recently we have used waste *M. acuminata* banana peel ash as a heterogeneous catalyst for sustainable production of biodiesel.<sup>31</sup>

With this interest, here we demonstrate the one pot green synthesis of a low cost, magnetically retrievable iron oxide ( $\text{Fe}_3\text{O}_4$ ) nanobase catalyst using banana (*M. acuminata*) peel ash extracts (hereafter denoted as MAPAE@ $\text{Fe}_3\text{O}_4$  NPs). Furthermore, the fabricated MAPAE@ $\text{Fe}_3\text{O}_4$  NP catalyst was characterized by various analytical and spectroscopic techniques. With our ongoing interest in the Henry reaction,<sup>33,34</sup> we further investigated its catalytic activity in the synthesis of  $\beta$ -nitroalcohol using nitroalkanes with different aldehydes and the results obtained are found to be excellent.

## 2 Experimental methodology

### 2.1 Preparation of MAPAE@ $\text{Fe}_3\text{O}_4$ NP catalysts

For the preparation of banana (*M. acuminata*) peel extracts, banana peels were collected and washed thoroughly with distilled water to remove impurities. These peels were then dried and burnt in open air to collect the ash. Now, 10 g of ash was dissolved in 100 mL of distilled water at 80 °C in a 500 mL round bottom flask and stirred for 1 h. The mixture was then filtered off and banana peel extracts were collected.

Magnetite nanoparticles ( $\text{Fe}_3\text{O}_4$  NPs) were prepared by a convenient co-precipitation method with slight modifications. Briefly, 5 mmol of  $\text{FeSO}_4 \cdot 7\text{H}_2\text{O}$  and 10 mmol of  $\text{FeCl}_3$  ( $\text{Fe}^{2+} : \text{Fe}^{3+} = 1 : 2$  molar ratio) were dissolved in 100 mL of deionized water at 90 °C. 20 mL *M. acuminata* banana peel ash extracts were then added to this solution dropwise with vigorous stirring. The colour of the solution became dark brown. After that a little amount of 1 M ammonia solution was added dropwise till the colour of the solution became completely dark. The synthesized  $\text{Fe}_3\text{O}_4$  NPs were allowed to settle and the solution was decanted. To this 50 mL of banana peel ash extract was again added and stirred for another half an hour. After that the water part of the solution was evaporated using a rotary evaporator and the dried solid nanocatalyst was collected and stored in a desiccator.

### 2.2 Characterization of MAPAE@ $\text{Fe}_3\text{O}_4$ NP catalysts

XRF, IR, XRD, XPS, SEM, TEM, EDX, VSM and TGA analyses were performed to evaluate the structure, composition and morphology of the synthesized nanoparticles. The FTIR spectra were recorded on KBr pellets using a Nicolet 6700 FTIR spectrophotometer. High resolution transmission electron microscopy (HRTEM) was recorded on an electron microscope (JEM-2100, 200 kV, JEOL). Energy dispersive X-ray spectroscopy (EDX) was also performed using the same instrument in EDX mode with a 0.28 sr solid angle (in a HR configuration with a 50 mm<sup>2</sup> detector). Powder X-ray diffraction (XRD) patterns were obtained on an X'Pert Pro PANalytical diffractometer under the following conditions: K-alpha1 wavelength  $\lambda = 1.54056$  Å, K-alpha2 wavelength  $\lambda = 1.54439$  Å, a generator voltage of 40 kV, a tube current of 35 mA and a count time of 0.5 s per 0.02° in the range of 5–90° with a copper anode. XPS analysis was carried out on an ESCALAB Xi<sup>+</sup>, Thermo Fisher Scientific instrument at room temperature. Magnetic measurements were carried out on a Lakeshore VSM 7410 magnetometer. The thermogravimetric analysis was carried out on a Perkin Elmer TGA 4000 instrument. The weight loss of the catalyst was recorded within a temperature range of 30–1000 °C, heating rate of 0.1–200 °C min<sup>−1</sup> under a constant flow of nitrogen gas. <sup>1</sup>H and <sup>13</sup>C NMR spectra of synthesized  $\beta$ -nitroalcohol were recorded on a Bruker Avance II (400 MHz), spectrometer using tetramethylsilane (TMS) as an internal reference.

### 2.3 General procedure for synthesis of $\beta$ -nitroalcohols

To a well-stirred mixture of aldehyde (1 mmol) and nitroalkane (1.5 mmol) in a sample vial, 50 mg of MAPAE@ $\text{Fe}_3\text{O}_4$  NPs was added at ambient temperature. The reaction mixture was allowed to stir for the time specified in Table 3. The progress of the reaction was monitored using TLC. After completion of the reaction (as indicated by TLC), the catalyst was isolated using an external magnet and the resultant mixture was purified by silica gel column chromatography to give the corresponding nitroalcohol.

### 2.4 Basicity measurement

The basic strength of the solid catalyst was determined by using the Hammett indicator method. The following Hammett indicators are used in our experiments: bromothymol blue ( $H_- = 7.2$ ), phenolphthalein ( $H_- = 9.8$ ), alizarin yellow R ( $H_- = 11.0$ ), indigo carmine ( $H_- = 12.2$ ), 2,4-dinitroaniline ( $H_- = 15.0$ ) and nitroaniline ( $H_- = 18.4$ ). Approximately 200 mg of solid catalyst and a 1 mL solution of the Hammett indicator diluted with 5 mL of anhydrous methanol was shaken and allowed to equilibrate for 2 h. If the solution exhibits a colour change it indicates that the basic strength of the catalyst is stronger than the strength of the indicator used. However, if the solution does not produce any colour change, it means that the basic strength of the catalyst is weaker than the indicator used.<sup>35</sup>

### 2.5 Catalyst recyclability test

To investigate the reusability of the catalyst, the catalyst was utilized for several consecutive cycles under our optimized



reaction conditions. Once the reaction was completed the catalyst was subjected to washing with methanol and hexane to remove any impurities. The washed catalyst was dried in a vacuum oven at 100 °C for 5 h and used for subsequent cycles.

## 3 Results and discussion

### 3.1 Catalyst characterization

To know the metallic and non-metallic compositions of the catalyst, XRF analysis was performed. Apart from  $\text{Fe}_3\text{O}_4$ , the  $\text{MAPAE@Fe}_3\text{O}_4$  NP catalyst was found to contain  $\text{K}_2\text{O}$  (46.24%) and  $\text{SiO}_2$  (22.35%) as major constituents for catalytic activation. Beside these, several other metal oxides such as  $\text{Al}_2\text{O}_3$ ,  $\text{CaO}$ ,  $\text{Na}_2\text{O}$ ,  $\text{P}_2\text{O}_5$ , and  $\text{MnO}$  are also found to be present in trace amounts. The presence of these metal oxides in the  $\text{MAPAE@Fe}_3\text{O}_4$  NP catalyst is responsible for its catalytic activity as a base in the Henry reaction.

To detect the functional groups present in the  $\text{MAPAE@Fe}_3\text{O}_4$  NP catalyst, IR analysis was performed (Fig. 1). The FT-IR spectra showed an intense peak at  $586\text{ cm}^{-1}$  corresponding to the Fe–O bond vibration which is the characteristic peak of  $\text{Fe}_3\text{O}_4$  nanoparticles. The peaks at  $3413\text{ cm}^{-1}$  and  $1640\text{ cm}^{-1}$  can be attributed to the –OH stretching and bending vibrations of the absorbed moisture over the catalyst surface. The absorption band at  $688\text{ cm}^{-1}$  may be assigned to the K–O and Ca–O stretching vibrations. The peak at  $1399\text{ cm}^{-1}$  may be due to the presence of a metal carbonate, *e.g.*  $\text{K}_2\text{CO}_3$ , in the catalyst. The two absorption bands at  $1117\text{ cm}^{-1}$  and  $791\text{ cm}^{-1}$  are the characteristic stretching and bending vibrations of the Si–O–Si bond, respectively.<sup>36</sup> The single band at  $886\text{ cm}^{-1}$  observed in the  $\text{MAPAE@Fe}_3\text{O}_4$  catalyst may be due to the vibration of isolated  $\text{SiO}_4$  in  $\text{M}^{2+}\text{SiO}_4$  perturbed by the interaction with  $\text{M}^{2+}$ .<sup>37</sup>

The crystalline structure of the  $\text{MAPAE@Fe}_3\text{O}_4$  NP catalyst was analyzed by XRD analysis (Fig. 2) and it was seen that the XRD peaks match very well with the characteristic peaks of the inverse cubic spinel structure of crystalline  $\text{Fe}_3\text{O}_4$  nanoparticles giving  $2\theta$  values of  $30.13$ ,  $33.73$ ,  $43.50$  and  $55.26^\circ$  (JCPDS file no.

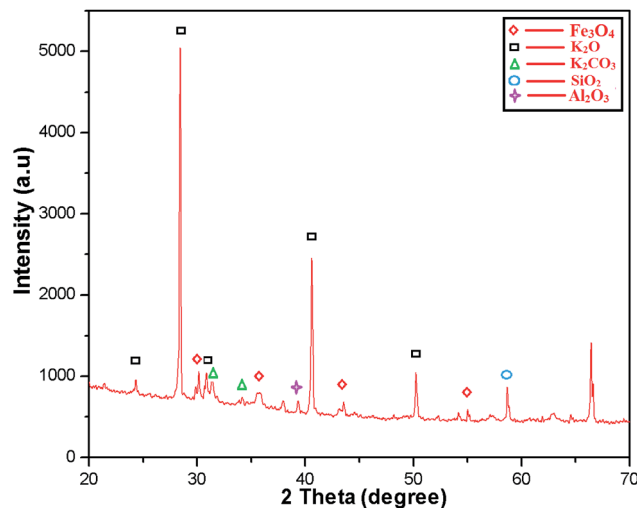


Fig. 2 XRD patterns of the  $\text{MAPAE@Fe}_3\text{O}_4$  NPs.

89-3854). The strong characteristic peaks of  $\text{K}_2\text{O}$  and  $\text{K}_2\text{CO}_3$  were also observed at  $2\theta = 28.44$ ,  $30.74$ ,  $31.52$ ,  $34.21$ ,  $40.49$ ,  $50.30^\circ$  (JCPDS reference file no. 77-2176 and 71-1466). The presence of  $\text{SiO}_2$  was also confirmed by the appearance of peaks at  $2\theta = 34.33$ ,  $57.44^\circ$  (JCPDS reference file no. 89-3609). Besides these, the peaks at  $2\theta = 38.00$  and  $66.47^\circ$  also indicated the presence of  $\text{Al}_2\text{O}_3$  in the catalyst.

The size, shape and surface morphology of the synthesized  $\text{MAPAE@Fe}_3\text{O}_4$  NPs were investigated by SEM and TEM analysis (Fig. 3). From the SEM images (Fig. 3a and b), it was clearly seen that the  $\text{Fe}_3\text{O}_4$  particles are covered with metal oxides and carbonates producing horizontal flake-like structures of different sizes and it is very difficult to determine the size of the particles due to the agglomeration of the particles. The TEM images of  $\text{MAPAE@Fe}_3\text{O}_4$  (Fig. 3c and d) revealed that the particles have core/shell structures and black colour shows  $\text{Fe}_3\text{O}_4$  and ash colour is for metal oxides and carbonates impregnated over  $\text{Fe}_3\text{O}_4$  surfaces which confirmed the formation of an outer layer over  $\text{Fe}_3\text{O}_4$  surfaces. The particles are

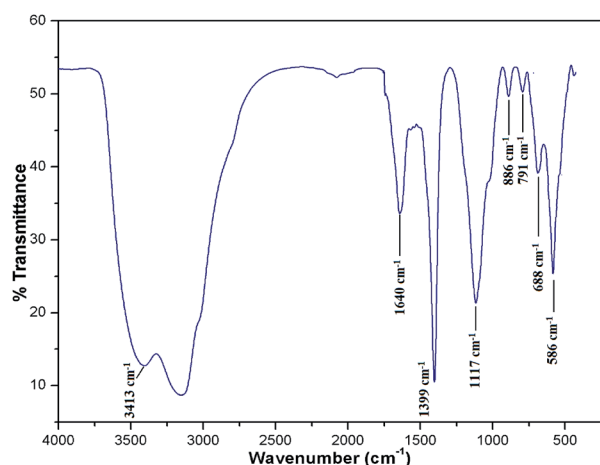


Fig. 1 FT-IR spectra of the  $\text{MAPAE@Fe}_3\text{O}_4$  catalyst.

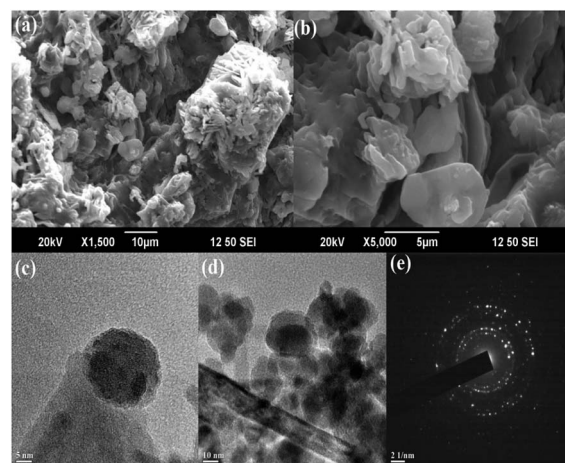


Fig. 3 (a and b) SEM images, (c and d) TEM images of  $\text{MAPAE@Fe}_3\text{O}_4$  nanoparticles at various magnifications, and (e) SAED pattern.



quasi-spherical in shape having diameters ranging from 20–30 nm. The SAED pattern (Fig. 3e) confirmed that the particles are polycrystalline in nature.

To investigate the surface composition of the synthesized nanoparticles, XPS analysis was performed as shown in Fig. 4. The wide scan XPS spectrum showed the presence of K 2p (27.56%) and O 1s (70.51%) as the major constituents and negligible amounts of Al 2p, Si 2p and P 2p are also present on the catalyst surface. The deconvoluted peaks of K 2p consist of two peaks with binding energies of 294.5 eV and 291.8 eV, which can be attributed to the presence of potassium as an oxide and carbonate on the catalyst surface.<sup>31</sup> There was only one peak at 530.5 eV in the O 1s spectrum, which indicated the presence of metal oxides. The Si 2p peak at 100.09 eV can be attributed to the presence of oxides of silicon on the catalyst surface.<sup>38</sup> The disappearance of the Fe 2p peak clearly indicated that the surfaces of Fe<sub>3</sub>O<sub>4</sub> nanoparticles are fully covered with metal oxides, which is responsible for its high basicity or high catalytic activity. The EDS analysis of the MAPAE@Fe<sub>3</sub>O<sub>4</sub> NP catalyst also supported the results of XPS analysis and revealed the presence of K, O, C and Fe in the catalyst (Fig. 5).

The occurrence of magnetic behavior for raw Fe<sub>3</sub>O<sub>4</sub> (collected before addition of extra ash extracts) and MAPAE@Fe<sub>3</sub>O<sub>4</sub> nanoparticles was confirmed by the closed *M*–*H* loop shown in Fig. 6. It can be seen that, in comparison with 64.65 emu g<sup>−1</sup> of Fe<sub>3</sub>O<sub>4</sub>, the saturation magnetization of MAPAE@Fe<sub>3</sub>O<sub>4</sub> was found to be 38.14 emu g<sup>−1</sup> after being impregnated with ash extracts. This may be due to the formation of an outer layer of metal oxides and carbonates over the surface of the Fe<sub>3</sub>O<sub>4</sub> core. Moreover, both the remanence and coercivity value are almost negligible suggesting that the

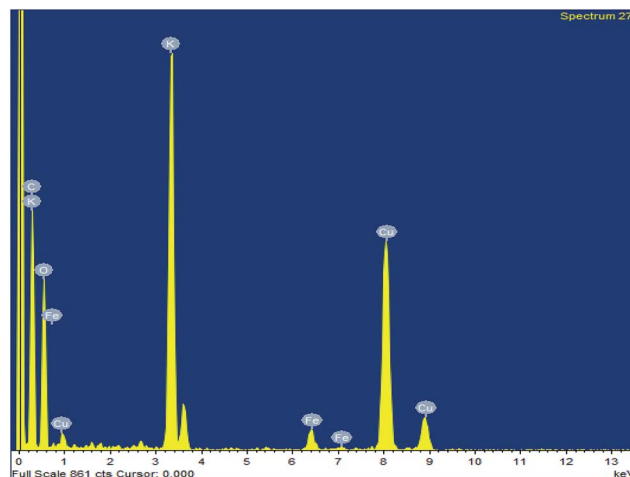


Fig. 5 EDX spectrum of the MAPAE@Fe<sub>3</sub>O<sub>4</sub> nanoparticles.

synthesized Fe<sub>3</sub>O<sub>4</sub> and MAPAE@Fe<sub>3</sub>O<sub>4</sub> nanoparticles are superparamagnetic in nature. TGA analysis was also performed to investigate the thermal stability of the MAPAE@Fe<sub>3</sub>O<sub>4</sub> catalyst (Fig. 7). In the TG curve, a 2–3% initial weight loss was observed at 50–180 °C due to removal of absorbed moisture. The weight loss between 200 and 450 °C may be due to the thermal decomposition of metal oxides and the oxidation of carbonaceous materials present in the catalyst to release CO, CO<sub>2</sub>, etc.

The basic strength of the MAPAE@Fe<sub>3</sub>O<sub>4</sub> NPs was also investigated by the Hammett indicator method according to the above mentioned procedure. From the experiment it was seen that when bromothymol blue and phenolphthalein solution were mixed with the catalyst, the colour of the solution changed

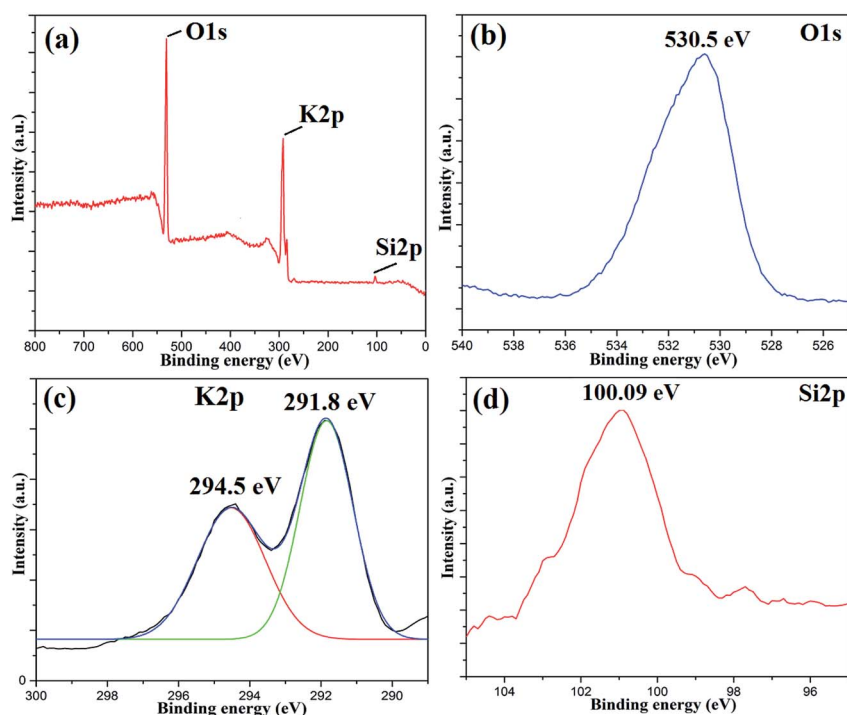


Fig. 4 (a) XPS survey spectrum, and (b) O 1s, (c) K 2p and (d) Si 2p spectra of MAPAE@Fe<sub>3</sub>O<sub>4</sub>.





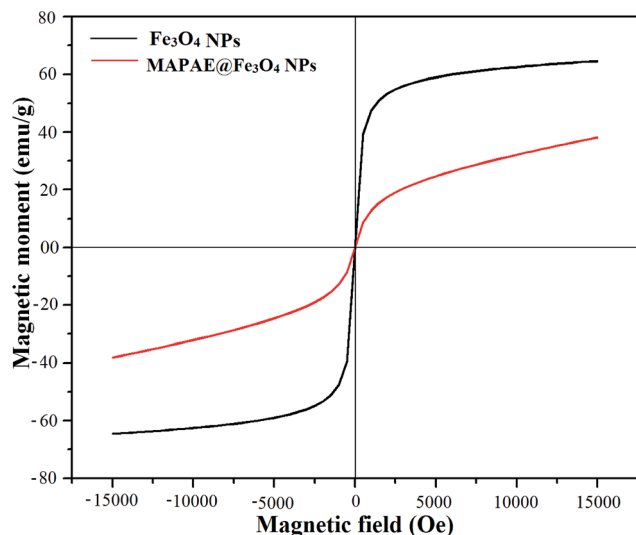


Fig. 6 The magnetic hysteresis loop of  $\text{Fe}_3\text{O}_4$  and  $\text{MAPAE}@\text{Fe}_3\text{O}_4$  NPs.

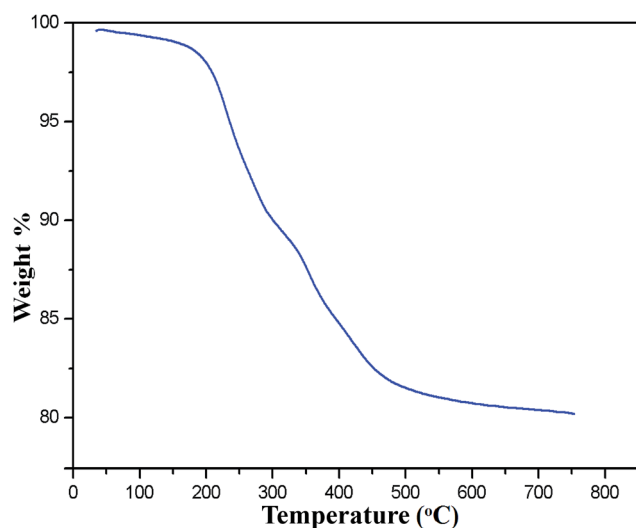


Fig. 7 TGA thermogram of  $\text{MAPAE}@\text{Fe}_3\text{O}_4$  NPs.

but when the alizarin yellow R indicator was used no colour change was observed. Therefore the basic strength of the catalyst could be tentatively denoted as  $9.8 < H_- < 11.0$ .

### 3.2 Henry reactions

At the beginning, with our prepared base catalyst we performed the Henry reaction of 4-nitrobenzaldehyde with nitromethane at room temperature under solvent free conditions as a pilot protocol. It was seen that the desired product  $\beta$ -nitroalcohol was formed without formation of a dehydrated byproduct within 70 min to generate 99% isolated yield (Scheme 1). Furthermore, optimization of various parameters like the catalyst amount and molar ratio of reactants was also investigated.

**Optimization of the catalyst amount.** To investigate the catalyst amount required for fast and complete conversion of the reactants, 4-nitrobenzaldehyde and nitromethane were



Scheme 1 Henry reaction of 4-nitrobenzaldehyde with nitromethane using the  $\text{MAPAE}@\text{Fe}_3\text{O}_4$  catalyst.

employed as test substrates with different masses of the nano-catalyst. Optimization of the catalyst loading is shown in Table 1. It was observed that with 50 mg of the catalyst the reaction took the least time to complete with an excellent yield of 99% in 70 min (Table 1, entry 3).

**Optimization of the molar ratio of the reactants.** The required molar ratio of the reagents by taking different equivalents of aldehyde and nitroalkane was also investigated and it was found that 1 mmol of aldehyde and 1.5 mmol of nitroalkane (*i.e.* 1 : 1.5) were most suitable for this reaction (Table 2).

With the optimized reaction conditions in hand, the reaction was further generalized to a variety of aldehydes to investigate the scope and limitations of our method and the results are summarized in Table 3. It was seen that the reaction of various aldehydes with nitroalkane was rapid and gave good to excellent yields in all cases with our synthesized base catalyst (Table 3, 3a–t). From the table it was seen that aromatic aldehydes with an electron withdrawing substituent like 4-nitrobenzaldehyde undergo faster reaction and gave better yields (Table 3 and 3c). However, less electrophilic aldehydes with electron donating groups such as 3,4,5-trimethoxybenzaldehyde (Table 3, 3i) gave a lower amount of yield. This may be due to the fact that electron withdrawing groups enhance the electrophilicity of the carbonyl carbon which facilitates the reaction while electron donating groups provide it with electrophilicity resulting in the lower percentage of yield.

Table 1 Optimization of the weight of the catalyst<sup>a</sup>

Entry	Amount (in mg)	Time (min)	Yield (%)
1	30	90	80
2	40	85	85
3	50	70	99
4	60	80	98

<sup>a</sup> Reaction conditions: 4-nitrobenzaldehyde (1 mmol), nitromethane (1.5 mmol), solvent free, room temperature.

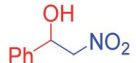
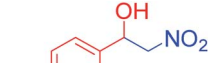
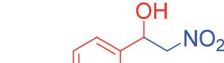
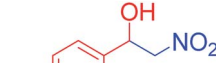
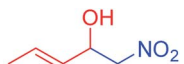
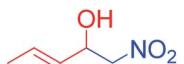
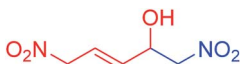
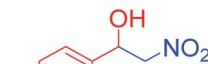
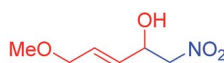
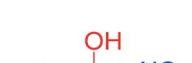

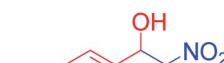
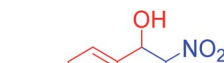
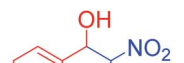
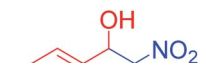
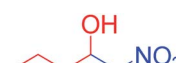
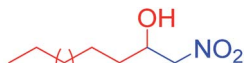
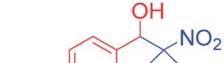
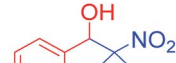
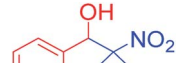
Table 2 Optimization of the molar ratio of reagents<sup>a</sup>

Entry	Aldehyde/nitroalkane	Time (min)	Yield (%)
1	1 : 1	85	90
2	1 : 1.5	70	99
3	1 : 2	80	92
4	2 : 1	85	56

<sup>a</sup> Reaction conditions: 4-nitrobenzaldehyde, nitromethane, catalyst:  $\text{MAPAE}/\text{Fe}_3\text{O}_4$  (50 mg), solvent free, room temperature.



Table 3 Henry reactions of various aromatic and aliphatic aldehydes with nitroalkane under solvent free conditions<sup>a</sup>

$  \begin{array}{c}  \text{O} \\  \parallel \\  \text{R}-\text{C}-\text{H} \quad \text{1} + \quad \text{R}^1-\text{CH}_2-\text{NO}_2 \quad \text{2} \\  \text{R} = \text{alkyl, aryl, R}^1 = \text{alkyl, H}  \end{array}  \xrightarrow[\text{SolIFC, RT}]{\text{MAPAE@Fe}_3\text{O}_4}  \begin{array}{c}  \text{OH} \\    \\  \text{R}-\text{C}-\text{CH}(\text{R}^1)-\text{NO}_2 \\  \text{3a-t}  \end{array}  $			
 <b>3a</b> , 90 m, 90%	 <b>3b</b> , 80 m, 94%	 <b>3c</b> , 70 m, 99%	 <b>3d</b> , 80 m, 94%
 <b>3e</b> , 78 m, 93%	 <b>3f</b> , 75 m, 97%	 <b>3g</b> , 75 m, 92%	 <b>3h</b> , 100 m, 75%
 <b>3i</b> , 114 m, 70%	 <b>3j</b> , 95 m, 90%	 <b>3k</b> , 98 m, 87%	 <b>3l</b> , 85 m, 94%
 <b>3m</b> , 82 m, 99%	 <b>3n</b> , 85 m, 95%	 <b>3o</b> , 75 m, 97%	 <b>3p</b> , 80 m, 90%
 <b>3q</b> , 85 m, 90%	 <b>3r</b> , 87 m, 97%	 <b>3s</b> , 92 m, 95%	 <b>3t</b> , 90 m, 94%

<sup>a</sup> Reaction conditions: aldehyde (1 mmol), nitromethane (1.5 mmol), MAPAE@Fe<sub>3</sub>O<sub>4</sub> NPs (50 mg) at room temperature.

We also found that reactions using aliphatic aldehydes were somewhat slower. This may be due to the electron donating tendency of the alkyl groups present in the chain (Table 3, **3j**, and **3k**). With the interest to know the effect of chain length and the substitution in the nitroalkane, we further investigated the reaction of aldehydes with nitroethane and 2-nitropropane under similar conditions. These reactions were also efficient and gave an excellent yield of nitroalcohol. It was seen that the substitution pattern in the aldehyde group affects the reaction in the same way as in the case of nitromethane but the reactions were slightly slower (Table 3, **3l–3t**). This can be attributed to the electronic effect and steric hindrance offered by the alkyl group present in the nitroalkane. FT-IR and NMR analysis of the synthesized compounds revealed the exclusive formation of nitroalcohol.

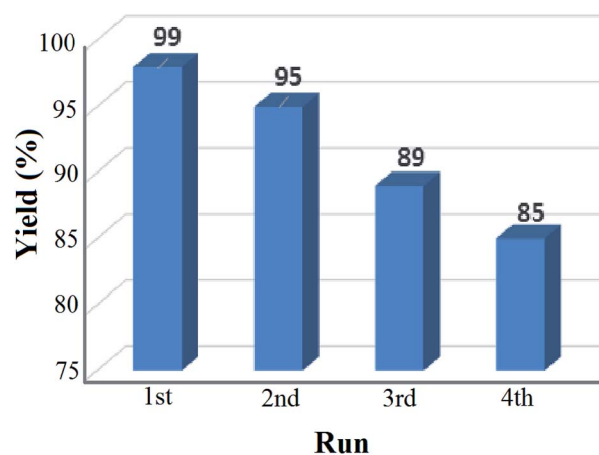


Fig. 8 Reusability of the MAPAE@Fe<sub>3</sub>O<sub>4</sub> catalyst for the Henry reaction.



### 3.3 Recyclability test of the catalyst

The reusability test for the solid base nanocatalyst was also studied under our optimized reaction conditions and the result is shown in Fig. 8. It was observed that the percentage of yield got reduced after repeated cycles and after the fourth cycle only 85% yield was recorded. This may be due to the leaching process of certain elements which can reduce the active sites of the catalyst resulting in the loss in catalytic activity. From the EDS analysis data of both the fresh and recovered catalyst after the fourth cycle, it was seen that there was a significant drop of the K concentration from 27.07% to 25.49% in the recovered catalyst (ESI, 2†). This significant loss in the K concentration of the fresh catalyst may affect the percentage yield of the product nitroalcohol in the second run. The XRD pattern of the recovered catalyst was almost similar to that of the fresh catalyst but the diffraction peaks have lower intensity than those of the fresh catalyst (ESI, 3†). The SEM and TEM images of the recovered catalyst also reveal the retention of the core/shell structure and polycrystalline nature of the nanoparticles (ESI, 3†).

## 4 Conclusion

In conclusion, we for the first time report the synthesis of a novel bio-waste derived solid base catalyst *i.e.* MAPAE@Fe<sub>3</sub>O<sub>4</sub> NPs using *M. acuminata* banana peel ash extracts and characterized them using various analytical techniques. The XRD and TEM results indicated that the synthesized catalyst is polycrystalline in nature having diameters ranging from 20–30 nm. The magnetic nanobase catalyst showed excellent catalytic activity for the synthesis of exclusively β-nitroalcohol *via* the Henry reaction at room temperature under solvent-free conditions. The metal oxides, predominantly K<sub>2</sub>O, form an outer layer over Fe<sub>3</sub>O<sub>4</sub> surfaces and are believed to be responsible for the high basicity of the catalyst. In addition, the catalyst exhibited a strong magnetic response and could be easily separated from the reaction mixture by simply applying an external magnet and reused for 4 consecutive cycles. The greenness of the catalyst coupled with the ease of this methodology promise huge potential for wide utility in the field of chemical synthesis.

## Conflicts of interest

There are no conflicts interest to declare.

## Acknowledgements

We thank the Science and Engineering Research Board (SERB), New Delhi for financial support (Grant No. SB/FT/CS-103/2013 and SB/EMEQ-076/2014). SAIF-NEHU (Shillong), Gauhati University and STIC, Cochin are acknowledged for analysis.

## References

- 1 F. A. Luzzio, *Tetrahedron*, 2001, **57**, 915–945.
- 2 C. Acharya, A. Achari and P. Jaisankar, *Tetrahedron Lett.*, 2018, 8–11.
- 3 M. Halder, P. Bhanja, M. M. Islam, A. Bhaumik and S. M. Islam, *New J. Chem.*, 2018, **42**, 11896–11904.
- 4 B. El-asaad, E. Métaay and M. Lemaire, *Mol. Catal.*, 2017, **435**, 76–81.
- 5 A. P. C. Ribeiro, Y. Y. Karabach, L. M. D. R. S. Martins, A. G. Mahmoud, M. Fatima, C. Guedes and A. J. L. Pombeiro, *RSC Adv.*, 2016, **6**, 29159–29163.
- 6 T. Menapara, R. Tak, E. Chinnaraja, R. I. Kureshy, P. Patel and N. H. Khan, *ChemistrySelect*, 2017, **2**, 4063–4067.
- 7 Y. Li, Y. Huang, Y. Gui, J. Sun, J. Li, Z. Zha and Z. Wang, *Org. Lett.*, 2017, **19**, 10–13.
- 8 D. Cantillo, M. M. Moghaddam and C. O. Kappe, *J. Org. Chem.*, 2013, **78**, 4530–4542.
- 9 B. Karimi, F. Mansouri and H. Vali, *Green Chem.*, 2014, **16**, 2587–2596.
- 10 R. B. N. Baig and R. S. Varma, *Chem. Commun.*, 2013, **49**, 752–770.
- 11 S. Kim, E. Kim and B. M. Kim, *Chem.-Asian J.*, 2011, **6**, 1921–1925.
- 12 R. Y. Hong, B. Feng, L. L. Chen, G. H. Liu, H. Z. Li, Y. Zheng and D. G. Wei, *Biochem. Eng. J.*, 2008, **42**, 290–300.
- 13 M. Liong, J. Lu, M. Kovichich, T. Xia, S. G. Ruehm, A. E. Nel, F. Tamanoi and J. I. Zink, *ACS Nano*, 2008, **2**, 889–896.
- 14 N. A. Frey, S. Peng, K. Cheng and S. Sun, *Chem. Soc. Rev.*, 2009, **38**, 2532–2542.
- 15 P. Xu, G. M. Zeng, D. L. Huang, C. L. Feng, S. Hu, M. H. Zhao, C. Lai, Z. Wei, C. Huang, G. X. Xie and Z. F. Liu, *Sci. Total Environ.*, 2012, **424**, 1–10.
- 16 A. Hu, G. T. Yee and W. Lin, *J. Am. Chem. Soc.*, 2005, **127**, 12486–12487.
- 17 X. Li, X. Wang, S. Song, D. Liu and H. Zhang, *Chem.-Eur. J.*, 2012, **18**, 7601–7607.
- 18 J. Xu, H. Yang, W. Fu, K. Du, Y. Sui, J. Chen, Y. Zeng, M. Li and G. Zou, *J. Magn. Magn. Mater.*, 2007, **309**, 307–311.
- 19 T. J. Daou, G. Pourroy, S. Begin-Colin, J. M. Greneche, C. Ulhaq-Bouillet, P. Legare, P. Bernhardt, C. Leuvre and G. Rogez, *Chem. Mater.*, 2006, **18**, 4399–4404.
- 20 M. E. Compeán-jasso, F. Ruiz, J. R. Martínez and A. Herrera-gómez, *Mater. Lett.*, 2008, **62**, 4248–4250.
- 21 S. Santra, R. Tapeç, N. Theodoropoulou, J. Dobson, A. Hebard and W. Tan, *Langmuir*, 2001, **17**, 2900–2906.
- 22 A. Morel, S. I. Nikitenko, K. Gionnet, A. Wattiaux, J. Lai-keehim, C. Labrugere, B. Chevalier, G. Deleris, C. Petitobis, A. Brisson and M. Simonoff, *ACS Nano*, 2008, **2**, 847–856.
- 23 L. Cabrera, S. Gutierrez, N. Menendez, M. P. Morales and P. Herrasti, *Electrochim. Acta*, 2008, **53**, 3436–3441.
- 24 J. K. Patra and K. Baek, *J. Photochem. Photobiol. B*, 2017, **173**, 291–300.
- 25 K. B. Narayanan and N. Sakthivel, *Adv. Colloid Interface Sci.*, 2010, **156**, 1–13.
- 26 A. Bharde, D. Rautaray, V. Bansal, A. Ahmad, I. Sarkar, S. M. Yusuf, M. Sanyal and M. Sastry, *Small*, 2006, **64**, 135–141.
- 27 W. Zhou, W. He, S. Zhong, Y. Wang, H. Zhao, Z. Li and S. Yan, *J. Magn. Magn. Mater.*, 2009, **321**, 1025–1028.



- 28 M. Mahdavi, F. Namvar, M. Bin Ahmad and R. Mohamad, *Molecules*, 2013, **18**, 5954–5964.
- 29 S. Venkateswarlu, Y. S. Rao, T. Balaji, B. Prathima and N. V. V. Jyothi, *Mater. Lett.*, 2013, **100**, 241–244.
- 30 P. D. Pathak, S. A. Mandavgane and B. D. Kulkarni, *Rev. Chem. Eng.*, 2016, **32**, 1–15.
- 31 G. Pathak, D. Das, K. Rajkumari and L. Rokhum, *Green Chem.*, 2018, **20**, 2365–2373.
- 32 P. Jamal, O. K. Saheed and Z. Alam, *Asian J. Biotechnol.*, 2012, **4**, 1–14.
- 33 D. Das, G. Pathak and L. Rokhum, *RSC Adv.*, 2016, **6**, 104154–104163.
- 34 L. Rokhum and G. Bez, *Can. J. Chem.*, 2013, **91**, 300–306.
- 35 H. Li, S. Niu, C. Lu, M. Liu and M. Huo, *Energy Convers. Manage.*, 2014, **86**, 1110–1117.
- 36 W. Deligeer, Y. W. Gao and S. Asuha, *Appl. Surf. Sci.*, 2011, **257**, 3524–3528.
- 37 E. Betiku, A. M. Akintunde and T. V. Ojumu, *Energy*, 2016, **103**, 797–806.
- 38 X. Yu, Y. Gong, W. Bi, X. Tian, H. Ma, H. Zhao, G. Qiu and L. Wang, *Key Eng. Mater.*, 2008, **368–372**, 1277–1279.

